Research on Optimization of Acoustic Packaging Performance of Electric Vehicle Motor Compartment Based on Transfer Matrix Theory

Jintao SU [1], Weizheng LIU [1], Nenghui HUANG [2 *]

[1] *College of Automotive and Electrical Engineering, Harbin Cambridge University, 239 Haping Road, Xiangfang District, Harbin 150000, Heilongjiang Province, China*
[2] *School of Mechanical and Automotive Engineering, Science and Technology College of Hubei University of Arts and Science, 296 Longzhong Road, Xiangcheng District, Xiangyang 441025, Hubei Province, China*

http://doi.org/10.5755/j02.ms.42507

Received 20 August 2025; accepted 31 October 2025

This study addresses the prevalent issue of inadequate low-frequency sound absorption within electric vehicle motor compartments by introducing a novel multi-layer composite acoustic structure characterized by a gradient flow resistance design, grounded in transfer matrix theory. An acoustic transmission model was developed, and the proposed design was evaluated through both simulation and experimental validation. Results indicate that the gradient flow resistance configuration enhances the sound absorption coefficient by 15 – 20 % compared to conventional single-layer materials within the 200 – 500 Hz low-frequency range, while achieving a sound absorption coefficient exceeding 0.9 at higher frequencies. Furthermore, the application of a simplified transfer matrix model reduces computational complexity by approximately 30 % without compromising accuracy. This research offers a pioneering design methodology for acoustic packaging solutions in electric vehicle motor compartments.
Keywords: electric vehicle, acoustic performance, transfer matrix method, multi-layer composite materials.

1. INTRODUCTION

With the rapid development of modern technology, acoustic materials play a crucial role in fields such as aerospace, the construction industry, and the automotive industry. The sound quality of electric vehicles has always been a hot topic in industry research. The multi-layer composite materials of the acoustic package for electric vehicles have attracted extensive attention from researchers at home and abroad due to the flexibility of their structural design and the ability to integrate the acoustic performance advantages of various materials, and have become one of the hotspots in the research of acoustic materials.

The research on the acoustic properties of multi-layer composite materials abroad started earlier and has formed a systematic theory and method. Biot, M.A. [1] proposed a theoretical model of sound wave propagation in porous materials in 1956, laying a theoretical foundation for subsequent simulation studies. Giulio, E.D. et al. [2] has refined the theoretical system of acoustic propagation transport parameters in air-saturated stationary porous materials on this basis. Zhang, Y. et al. [3] systematically studied the structural design and performance optimization of composite acoustic insulating metamaterials and proposed a variety of innovative designs. Sagomonova, V.A. et al. [4] optimized the composition and structure of composite materials with enhanced vibration absorption characteristics through experiments. Qi, M. et al. [5] studied the problem of low-frequency noise in the rocket fairing and proposed a noise reduction mechanism. Zheng, Z. et al. [6] studied the acoustic radiation performance of the double-wall cylindrical shell structure, improved the accuracy of sound field prediction, and provided theoretical support for low-noise design. Deng, X. [7] studied the structural acoustic characteristics of an internal combustion engine and its optimization design method, and carried out the verification of the noise reduction scheme. Since the rise of structural vibration and radiated noise correlation mechanism research, the acoustic package optimization technology has been breaking through. The synergistic application of multi-physical field coupling simulation and topology optimization technology has become the focus of the research, and the precise regulation is realized through the analysis of the acoustic vibration transmission path and optimization of material parameters. Yang, X. et al. [8] conducted a systematic analysis of the sound insulation performance of composite rubber filled with glass microspheres. Research has found that by adjusting parameters such as the diameter, volume ratio, hollow ratio of hollow glass microspheres, and the thickness of composite rubber, the sound insulation effect can be effectively improved. Among them, thickness is a key factor affecting sound insulation performance. The core role of viscoelasticity and internal damping characteristics has been confirmed. Fig. 1 illustrates the design of the acoustic package for the front cover of an electric vehicle's motor compartment, encompassing both the front cover and the sound-absorbing materials utilized.

Although China started late, it has also made significant progress. Yang, Z. et al. [9] studied the influence of various structural parameters on sound absorption performance and improved the sound absorption performance of multilayer composite materials in the low frequency range.

* Corresponding author: N. Huang
E-mail: *11947@hbuas.edu.cn*

Ma, Z. et al. [10] studied the low-frequency noise reduction technology of flexible acoustic metamaterials. Qi, M. et al. [11] proposed a composite sound-absorbing structure, which overcomes the defect of the limited frequency band of a single material.

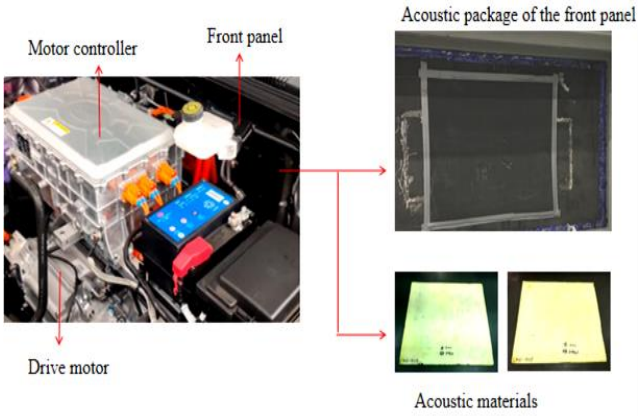

Fig. 1. Acoustic package structure of the power compartment of an electric vehicle

Zhang, B. et al. [12] conducted a systematic optimization design of the structural parameters of the acoustic cover layer in cylindrical cavities, providing a theoretical basis for the improvement of the acoustic stealth performance of underwater equipment. Chen, Y. et al. [13] have provided an important theoretical basis for the design and application of new lightweight sound insulation materials through the study of sandwich structures based on negative Poisson's ratio structures. Xiong, X. [14] through the testing and research on the acoustic performance of automotive porous sound-absorbing materials, the significant influence of material porosity, thickness and structural parameters on sound absorption performance was revealed, providing a theoretical and experimental basis for automotive noise control. Chen, H. et al. [15] conducted a simulation study on the load-bearing and vibration performance of water-lubricated tail bearing systems based on acoustic metamaterials, revealing the significant role of acoustic metamaterials in optimizing the load-bearing capacity and vibration suppression of tail bearing systems. This provides new theoretical support and a practical basis for the low-noise and high-stability design of ship propulsion systems. Zu, X. et al. [16] by establishing an effective theoretical model, revealed the acoustic vibration response law of fiber/resin sandwich panels with porous foam cores. He found that the core layer parameters and structural dimensions have a significant impact on their vibration, sound radiation, and sound transmission loss, providing a theoretical basis for the optimal design of this type of structure in the field of sound insulation. Chen, W. et al. [17] revealed through theoretical analysis and numerical simulation the close relationship between the sound absorption performance of porous metal materials and their porosity, thickness, and microstructure geometry. Sun, W. et al. [18] studied the acoustic properties of polyurethane/epoxy resin elastomers through simulation and experiments, revealing the significant influence of elastic modulus, loss factor, and Poisson's ratio on the sound absorption performance of the material, providing a theoretical basis for the design and optimization of underwater acoustic sound-absorbing materials. Lv, L. et al. [19] revealed the key influence of the dynamic mechanical parameters of viscoelastic materials on their dynamic response characteristics, and elucidated the correlation mechanism between these parameters and the acoustic performance of the cover layer, which provides theoretical support for the enhancement of the acoustic design of underwater acoustic materials.

Despite notable advancements in acoustic materials research within the domains of aviation and architecture, there remains a considerable deficiency in focused investigations addressing high-frequency noise and low-frequency resonance issues specifically related to electric vehicle motor compartments. To address the existing research gap, this study focuses on the front panel of the motor compartment in electric vehicles. It develops an acoustic transmission model for multilayer composites utilizing transfer matrix theory and conducts a comprehensive analysis of the mechanisms by which parameters such as porosity and flow resistivity affect acoustic performance. The findings aim to offer a theoretical foundation and parametric guidance for the optimal design of acoustic packaging within the motor compartment.

This research introduces a novel modeling approach grounded in transfer matrix theory, which significantly streamlines the computational process associated with high-frequency acoustic performance. Furthermore, this method effectively mitigates the systematic errors arising from the nonlinear properties of material parameters, in contrast to conventional finite element analysis. The study is centered on three primary objectives: to develop a theoretical model for the transfer matrix of multilayer composite materials and to validate this model through experimental methods; to conduct a comprehensive analysis of the mechanisms by which critical material parameters affect acoustic performance; and to formulate an optimized design strategy aimed at mitigating low-frequency noise within the engine compartment of electric vehicles. The research methodology encompasses the development of an acoustic model for multilayer composites utilizing transfer matrix theory. It further involves the integration of numerical simulations with impedance tube experiments to investigate the effects of various parameters on the sound absorption coefficients and impedance coefficients. The transfer matrix method offers considerable benefits in comparison to the conventional finite element method (FEM) and boundary element method (BEM). Guo, R. et al. [20] demonstrated that while the finite element method is proficient in accurately simulating the acoustic performance of intricate structures, it is characterized by significant computational complexity, particularly in high-frequency analyses. This method necessitates substantial meshing and computational resources. While the boundary element method (BEM) is highly effective for addressing issues related to infinite domains, research conducted by Chen, J.T. [21] indicates that, despite advancements in algorithms such as the double boundary element method, BEM continues to encounter challenges related to low computational efficiency and difficulties in conducting parameter sensitivity analyses when applied to multilayer composites. These limitations hinder its capacity to facilitate parameter optimization and rapid design iterations for multilayer composite materials.

In contrast, the transfer matrix method mitigates computational complexity by converting the acoustic problem into a sequence of linear matrix operations, all the while maintaining a high level of predictive accuracy, exemplified by an error margin of less than 5 % in the absorption coefficient within the frequency range of 2000 Hz. Jie Chen's research indicates that the transfer matrix method demonstrates superior computational efficiency and greater convenience in parameter optimization compared to the boundary element method when addressing acoustic problems in layered media. This advantage renders it especially appropriate for the automotive sector's accelerated iterative design process, facilitating swift prototyping and parameter optimization to accommodate stringent product development timelines. Additionally, the validity of the model is assessed through univariate control experiments, which serve to furnish empirical data that supports optimal design considerations.

The findings of this research offer significant theoretical support for the acoustic packaging design of electric vehicles. Furthermore, they establish a methodological framework for future investigations into gradient flow resistivity characterization and multi-scale coupling simulation. This is particularly important for advancing the engineering application of multilayer composites in the acoustic management of electromechanical nacelles.

2. ACOUSTIC PERFORMANCE TRANSFER IN THE CABIN OF ELECTRIC VEHICLES

2.1. Transfer matrix model of monolayer porous materials

The transfer matrix method is the main approach for studying the acoustic characteristics of multilayer media. The formula [22] given in the literature for representing the transfer relationship between the sound pressure on the front and back surfaces of the material layer and the particle velocity using the transfer matrix is as follows [22]:

$$\begin{bmatrix} p \\ v \end{bmatrix}_{x=x_1} = \mathbf{T} \begin{bmatrix} p \\ v \end{bmatrix}_{x=x_2}, \tag{1}$$

where p is the surface sound pressure of the single-layer structure; v is the velocity of the particle; T is the transfer matrix of a single-layer structure; x_1, x_2 are the front and back positions of sound waves entering and leaving the surface of a single-layer structure, respectively.

As shown in Fig. 2, there are incident sound waves p_1 and reflected sound waves p_2 inside the porous material. In accordance with the principles of plane wave theory, the sound pressure and the associated particle velocity for these two waves are given by the following expressions, respectively:

$$p_1(x,t) = p_{1a}\exp\left(j\left(wt-kx\right)\right); \tag{2}$$

$$v_1(x,t) = \frac{p_{1a}}{Z_c}\exp\left(j\left(wt-kx\right)\right); \tag{3}$$

$$p_2(x,t) = p_{2a}\exp\left(j\left(wt+kx\right)\right); \tag{4}$$

$$v_2(x,t) = -\frac{p_{2a}}{Z_c}\exp\left(j\left(wt+kx\right)\right), \tag{5}$$

where Z_c is the characteristic impedance of the material; k is the wave number; ω is the angular frequency; p_1, p_2 are the amplitudes of the sound pressure of the incident wave and the reflected wave.

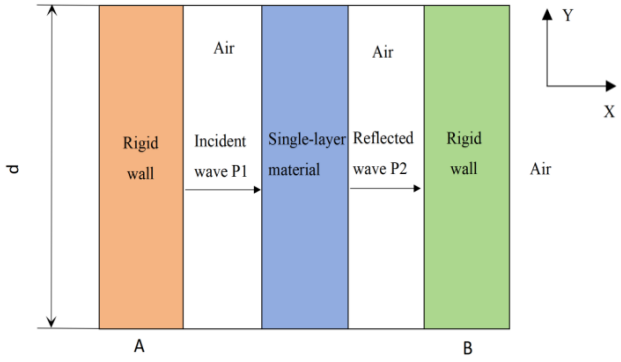

Fig. 2. Schematic diagram of the transfer matrix

Then the total sound pressure and particle velocity of the sound wave at a certain point in the material are, respectively:

$$p(x,t) = p_{1a}\exp\left(j\left(wt-kx\right)\right) + p_{2a}\exp\left(j\left(wt+kx\right)\right); \tag{6}$$

$$\mathbf{v}(x,t) = \frac{p_{1a}}{Z_c}\exp\left(j\left(wt-kx\right)\right) - \frac{p_{2a}}{Z_c}\exp\left(j\left(wt+kx\right)\right). \tag{7}$$

The sound pressure and particle velocity at points A and B are respectively expressed as

$$p(x_A,t) = p_{1a}\exp\left(j\left(wt-kx_A\right)\right) + p_{2a}\exp\left(j\left(wt+kx_A\right)\right); \tag{8}$$

$$v(x_A,t) = \frac{p_{1a}}{Z_c}\exp\left(j\left(wt-kx_A\right)\right) - \frac{p_{2a}}{Z_c}\exp\left(j\left(wt+kx_A\right)\right); \tag{9}$$

$$p(x_B,t) = p_{1a}\exp\left(j\left(wt-kx_B\right)\right) + p_{2a}\exp\left(j\left(wt+kx_B\right)\right); \tag{10}$$

$$v(x_B,t) = \frac{p_{1a}}{Z_c}\exp\left(j\left(wt-kx_B\right)\right) - \frac{p_{2a}}{Z_c}\exp\left(j\left(wt+kx_B\right)\right). \tag{11}$$

The above equation can be written in the form of a matrix:

$$\begin{bmatrix} p(x_A,t) \\ v(x_A,t) \end{bmatrix} = \begin{bmatrix} 1 & 1 \\ \frac{1}{Z_c} & -\frac{1}{Z_c} \end{bmatrix} \begin{bmatrix} p_{1a}\exp\left(j\left(wt-kx_A\right)\right) \\ p_{2a}\exp\left(j\left(wt+kx_A\right)\right) \end{bmatrix}. \tag{12}$$

The aforementioned transfer matrix delineates the transfer relationship between the acoustic pressure at the front and rear surfaces and the particle velocity as the acoustic wave traverses the porous medium. The fundamental objective of deriving Eq. 12 – Eq. 16 is to elucidate the phase transition of acoustic wave propagation within the material through the principle of phase superposition. This approach facilitates the conversion of the interference effects arising from incident and reflected waves into trigonometric expressions represented in a matrix format.

$$\begin{bmatrix} p(x_B,t) \\ v(x_B,t) \end{bmatrix} = \begin{bmatrix} \exp(jkd) & \exp(jkd) \\ \dfrac{\exp(jkd)}{Z_c} & -\dfrac{\exp(jkd)}{Z_c} \end{bmatrix} \begin{bmatrix} p_{1a}\exp\left(j\left(wt-kx_B\right)\right) \\ p_{2a}\exp\left(j\left(wt+kx_B\right)\right) \end{bmatrix}. \quad (13)$$

The derivation of Eq. 13 is grounded in the principle of phase superposition governing sound propagation in a single-layer porous medium. By representing the interference between incident and reflected waves through a matrix-based trigonometric formulation, the equation characterizes the phase delay experienced by sound waves within the material. This formulation is derived from the classical theoretical framework that relates sound pressure to sound velocity transmission in single-layer media within the context of acoustic transmission theory.

For the porous material, the thickness is defined as $d = x_{\mathrm{B}} - x_{\mathrm{A}}$. Substituting Eq. 12 into Eq. 13, the relationship between the sound pressure and the particle velocity at points A and B is obtained as follows:

$$\begin{bmatrix} p(x_A,t) \\ v(x_A,t) \end{bmatrix} = \mathbf{T} \begin{bmatrix} \mathrm{p}(x_B,t) \\ v(x_B,t) \end{bmatrix}. \quad (14)$$

From the above various forms, it can be obtained:

$$\begin{bmatrix} 1 & 1 \\ \dfrac{1}{Z_c} & \dfrac{1}{Z_c} \end{bmatrix} = \mathbf{T} \begin{bmatrix} \exp(jkd) & \exp(jkd) \\ \dfrac{\exp(jkd)}{Z_c} & \dfrac{\exp(jkd)}{Z_c} \end{bmatrix}. \quad (15)$$

The final transfer matrix formula expression obtained through simplification and organization is as follows

$$\mathbf{T} = \mathbf{T}_i \begin{bmatrix} \cos kd & jZ_c \sin kd \\ \dfrac{jZ_c \sin kd}{Z_c} & \cos kd \end{bmatrix}. \quad (16)$$

The final expression of the transfer matrix incorporates the terms cos(*kd*) and sin(*kd*), which represent the phase-delay effect of the acoustic wave as it travels through the material. When the product of the wave number *k* and the material thickness *d* equals an integer multiple of π, standing waves are established at the front and back surfaces of the material, leading to maximal values of the acoustic pressure amplitude. In contrast, the characteristic impedance *Z* serves to regulate the amplitude coupling between the acoustic pressure and the velocity of the plasma.

The transmission matrix model for single-layer materials is predicated on the fundamental parameters of characteristic impedance (*Z*) and wave number (*k*). Its derivation relies on the assumption of plane wave propagation and the linear uniformity of material parameters. In contrast to the multi-layer material transmission matrix model, the current model focuses solely on the relationship between sound pressure and vibration velocity transmission within a singular medium. This approach simplifies the boundary conditions to those of plane wave propagation against a rigid backing, thereby reducing computational complexity. Nevertheless, this model is limited in its capacity to represent the multi-level sound energy dissipation mechanisms inherent in multi-layer structures, as well as the interference effects of sound waves resulting from impedance mismatches between layers. Additionally, it fails to account for the impact of interlayer coupling on sound energy dissipation.

2.2. Multilayer composite porous material transfer matrix model

The transfer matrix formulation for multilayer composite porous materials must account for interlayer acoustic boundary matching conditions. Building upon the single-layer transfer matrix framework, a generalized multilayer transmission matrix model is established through enforcing interlayer continuity conditions and constructing global matrix connectivity, particularly suited for graded impedance structures. For the porous structure model as shown in Fig. 3, for the front and rear surfaces of the same layer of material, Eq. 1 and Eq. 16 can be expressed as [22]:

$$\begin{bmatrix} p_{2i-1} \\ v_{2i-1} \end{bmatrix} = \mathbf{T}_i \begin{bmatrix} p_{2i} \\ v_{2i} \end{bmatrix}; \quad (17)$$

$$\mathbf{T}_i = \begin{bmatrix} \cos k_i d_i & jZ_c \sin k_i d_i \\ \dfrac{j \sin k_i d_i}{Z_i} & \cos k_i d \end{bmatrix}; \quad (18)$$

$$Z_i = \sqrt{\rho_i k_i}\ ; \quad (19)$$

$$k_i = \omega \sqrt{\frac{\rho_i}{k_i}}\ , (20)$$

where $[p_{2i-1},\ v_{2i-1}]^{\mathrm{T}}$ and $[p_{2i},\ v_{2i}]^{\mathrm{T}}$ are respectively the sound pressure – particle velocity vectors at the inner and outer boundaries of the *i*-th layer material; ω is the angular frequency of the incident wave; d_i is the thickness of the *i*-th layer material; Z_i is the characteristic impedance of the *i*-th layer material; ρ_i and k_i are respectively the equivalent density and equivalent volumetric elastic modulus of the *i*-th layer material.

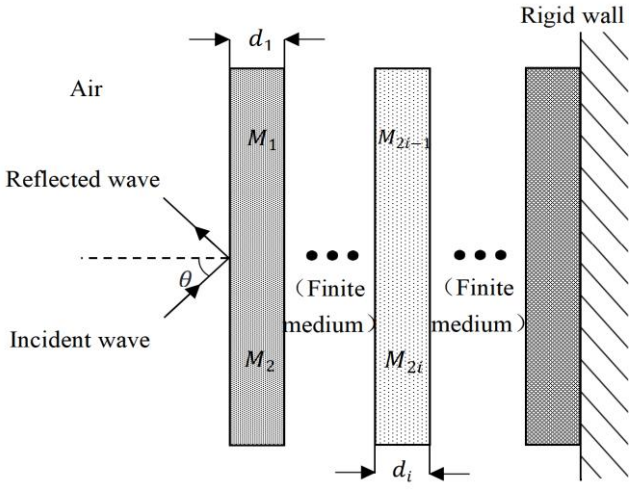

Fig. 3. Schematic diagram of multilayer composite porous materials

For the interface between two adjacent layers of materials, it can be obtained from the acoustic boundary conditions of continuous sound pressure and continuous volume velocity.

$$p_{2i} = p_{2i+1}; \tag{21}$$

$$\varphi_i v_{2i} = \varphi_{i+1} v_{2i+1}, \tag{22}$$

where p_{2i} and p_{2i+1} represent the sound pressures at the interface between two adjacent material layers respectively; v_{2i}, v_{2i+1}, are respectively the normal particle vibration velocities at the interface between two adjacent materials; φ_i, φ_{2i+1} represent the porosity of the i-th layer and the I + 1st layer of porous materials respectively.

Rewrite Eq. 17 in the form of a matrix to obtain it

$$\begin{bmatrix} p_{2i} \\ v_{2i} \end{bmatrix} = [\varphi_i] \begin{bmatrix} p_{2i+1} \\ v_{2i+1} \end{bmatrix} = \begin{bmatrix} 1 & 0 \\ 0 & \dfrac{\varphi_{i+1}}{\varphi_i} \end{bmatrix} \begin{bmatrix} p_{2i+1} \\ v_{2i+1} \end{bmatrix}. \tag{23}$$

For the outermost layer of the first material, that is, the interface with the outermost layer of air, the following relationship exists:

$$\begin{bmatrix} p_0 \\ v_0 \end{bmatrix} = [\varphi_i] \begin{bmatrix} p_{2i+1} \\ v_{2i+1} \end{bmatrix} = \begin{bmatrix} 1 & 0 \\ 0 & \dfrac{\varphi_{i+1}}{\varphi_i} \end{bmatrix} \begin{bmatrix} p_{2i+1} \\ v_{2i+1} \end{bmatrix}. \tag{24}$$

Among them, $[p_0, v_0]^T$ is the sound pressure-particle velocity vector on the outermost side of the first layer, i.e., the air side; φ_1 is the porosity of the first layer of porous material. The total transfer matrix of the multi-layer composite porous sound-absorbing material is

$$\mathbf{T_n} = \begin{bmatrix} 1 & 0 \\ 0 & j_1 \end{bmatrix} \prod_{i=1}^{n-1} \mathbf{T}_i [\varphi_i]_n = \begin{bmatrix} a_{11} & a_{12} \\ a_{21} & a_{22} \end{bmatrix}. \tag{25}$$

The transfer matrices of the outermost side of the first layer of material and the innermost side of the last layer of material are

$$\begin{bmatrix} p_0 \\ v_0 \end{bmatrix} = \mathbf{T}_n \begin{bmatrix} p_n \\ v_n \end{bmatrix}. \tag{26}$$

For the inner side of the last layer of material, since the backing of the composite material is a rigid wall surface, the sound wave undergoes total reflection at the interface. Therefore, the incident wave particle velocity v_{n1} and the reflected wave particle velocity v_{n2} are equal in magnitude but opposite in phase. As a result, the composite particle velocity at the interface is zero. It can be obtained by solving Eq. 17 and Eq. 26 simultaneously

$$\begin{bmatrix} p_0 \\ v_0 \end{bmatrix} = \begin{bmatrix} a_{11} p_n \\ a_{21} v_n \end{bmatrix}. \tag{27}$$

Then the surface acoustic impedance rate of the multi-layer composite porous material is

$$Z_s = \frac{p_0}{v_0} = \frac{a_{11}}{a_{21}}. \tag{28}$$

The sound absorption coefficients of multi-layer composite porous materials can be obtained by the following formula [22]

$$\alpha = 1 - \left| \frac{Z_s - \rho_0 c_0}{Z_s + \rho_0 c_0} \right|^2 = 1 - \left| \frac{a_{11} - a_{21} \rho_0 c_0}{a_{11} + a_{21} \rho_0 c_0} \right|^2. \tag{29}$$

From the above derivation, it can be seen that as long as the d_i, ρ_i, k_i of each layer of material is known, the overall transfer matrix of the multi-layer composite porous material can be derived, which subsequently allows for the determination of the sound absorption coefficients of the multi-layer composite porous material. The thickness of the material d_i can be directly measured. The equivalent density ρ_i and the equivalent volumetric elastic modulus k_i can be obtained through the Johnson-Champoux-Allard model. The multi-layer transmission matrix model developed in this study exhibits a simpler structural framework, enhanced computational accuracy, and greater efficiency relative to conventional finite element-based transmission matrix approaches. Unlike traditional methods, it obviates the need for constructing intricate finite element models and mitigates system errors arising from the absence of nonlinear material parameter characterization, thereby rendering it especially suitable for high-frequency acoustic performance analysis. The model operates under the assumptions of negligible lateral acoustic coupling between material layers and uniformly distributed porosity. Although these assumptions may neglect localized material inhomogeneities, future refinements incorporating statistical distribution functions hold potential to improve predictive accuracy in the low-frequency regime.

Firstly, the model elucidates the mechanisms by which critical parameters, such as porosity and flow resistivity, affect acoustic performance, thereby establishing a theoretical foundation for the design of experimental variables. Secondly, the model's computational efficiency facilitates the rapid optimization analysis of multiple parameters, as discussed in Section 4. Lastly, the alignment of experimental outcomes with model predictions serves to validate the accuracy of this approach and reinforces the model's reliability in informing the acoustic design of multi-layer composite materials.

A detailed elucidation of the primary symbols utilized in the formula is presented in Table 1.

Table 1. Main symbol table

Symbol	Definition	Unit	Physical meaning
p	Sound pressure	Pa	The sound pressure amplitude at the material's surface
v	Velocity of vibration	m/s	The speed of oscillation of a mass in the direction of the propagation of a sound wave
T	Transfer matrix	–	Matrix representing the relationship between sound pressure and velocity transfer
Z	Characteristic impedance	Pa·s/m	The impedance characteristics of materials in relation to acoustic waves
k	Wave number	rad/m	Demonstrating the spatial periodicity inherent in sound waves
ω	Angular frequency	rad/s	Demonstrating the temporal periodicity inherent in sound waves
d	Thickness	m	Thickness of single or multi-layer materials
σ	Flow resistivity	Pa·s/m^2	The resistivity to fluid flow per unit thickness of a material
φ	Porosity	–	The ratio of pore volume within the material

3. EXPERIMENTAL RESEARCH METHODS FOR COMPOSITE MATERIALS IN THE MOTOR COMPARTMENT

3.1. Experimental purpose and material selection

This experiment uses the impedance tube test method to systematically study the sound absorption performance of multi-layer composite acoustic materials composed of glass wool and foam materials. Glass wool demonstrates superior sound absorption capabilities in the high-frequency spectrum, attributable to its high porosity (0.99) and stable material properties, which facilitate parametric comparative analyses. Conversely, foam materials integrate elastic characteristics with a porous architecture. When these foam materials are combined with glass wool, they create a gradient flow resistivity distribution that effectively mitigates the sound absorption limitations of conventional materials in the low-frequency range. This study aims to investigate the influence mechanisms of critical parameters, including porosity, flow resistivity, and tortuosity, to validate the efficacy of gradient flow resistivity design in improving sound absorption performance within the low-frequency domain.

3.2. Experimental setup and test methods

The experimental methods for the acoustic properties of materials in the air mainly include the reverberation chamber method and the impedance tube method. According to the actual situation, this experiment adopts the impedance tube method to test the acoustic performance parameters of multi-layer composite materials under different parameter conditions. This testing method requires a small specimen area, so the installation and measurement are relatively convenient, and the testing accuracy can meet the requirements of scientific research. It is generally carried out in the impedance tube, as shown in Fig. 4, Fig. 5, Fig. 6.

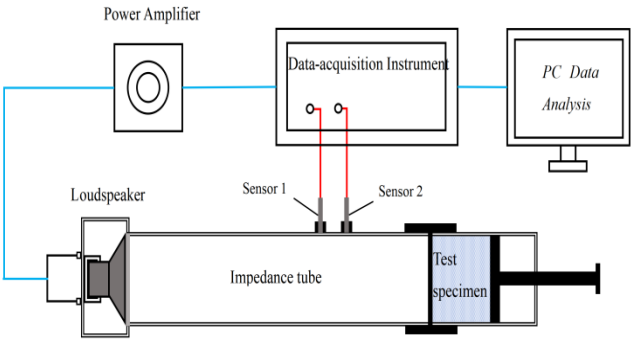

Fig. 4. Schematic diagram of the impedance tube experiment principle

The measurement was conducted using a dual-microphone impedance tube following ISO 10534-2, with a sample diameter of 29 mm and a test frequency range of 10 – 7000 Hz. One end of the impedance tube is a plane wave sound source. The sound diffuses after passing through the material to be tested through the speaker. The data acquisition instrument uses sensors to collect the sound wave information in the impedance tube and convert it into an electrical signal. Through post-processing of the data by computer software, the sound absorption coefficients of the material can be obtained.

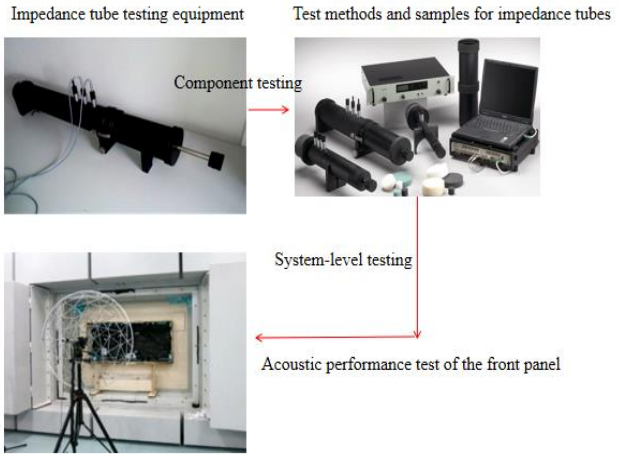

Fig. 5. Component testing and system testing methods for acoustic package materials

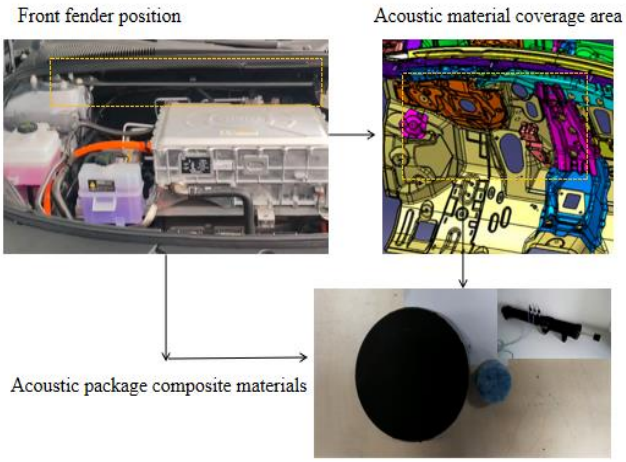

Fig. 6. Schematic diagram of the acoustic component test in the motor compartment

Since there is a certain functional relationship between the sound absorption coefficients of the sound-absorbing material and its impedance, the impedance of the material can also be obtained.

3.3. Experimental results and multivariate variable analysis

The test results of the composite materials for the cabin front panel are shown in Table 2.

Table 2. Experimental results

Material parameter	Porous flexible glass wool	Foam-8.8 kg/m^3
Porosity	0.99	0.99
Flow resistivity	9000	10900
Tortuosity	1.0	1.02
Viscous characteristic length, m	1.92×10^{-4}	1×10^{-4}
Thermal characteristic length, m	3.84×10^{-4}	1.3×10^{-4}
Solid density, kg·m^3	16	8.8
Poisson ratio	0	0.4
Young's modulus, N·m^2	4.4×10^{5}	8×10^{4}
Damping	0.1	0.17

The variable design of materials is carried out based on the test results. The design variables of the material, porosity, are 0.99, 0.5, and 0.3 respectively; the flow resistivities are 9000, 5000, and 20000 respectively; the tortuosity is 1.0, 1.5, and 3.0 respectively; and the viscosity characteristic lengths are 0.192 mm, 0.5 mm, and 1.0 mm respectively. The emission and reception sound domains are set to air, and the sound wave frequency is set to 10 – 7000 Hz. Based on the transfer matrix method, the excitation type is plane wave excitation.

Potential errors that may arise during the experimental process include dimensional discrepancies, such as deviations exceeding 0.1 mm in the cutting and mounting of samples, which can alter the boundary conditions. Additionally, phase calibration errors in the low-frequency range of impedance tube transducers can impact the temporal synchronization of acoustic pressure signals. Furthermore, variations in ambient temperature and humidity, particularly temperature fluctuations greater than 2°C, can affect the speed of sound, thereby leading to inaccuracies in the calculation of the sound absorption coefficients. For instance, with an air layer thickness of 15 mm, the deviation of the actual reflection coefficients at 310 Hz from their theoretical value can reach 0.03, which remains within the acceptable uncertainty of ± 5 % as stipulated by the ISO 10534-2 standard. To mitigate the impact of these errors on experimental outcomes, it is advisable to average results over multiple trials, optimize the sample installation procedure, and implement real-time compensation for temperature and humidity variations.

Since the amplitude, phase, incident Angle, excitation type, layer spacing and number of layers of the excitation wave are external factors and uncontrollable, only the influencing factors of the material itself, such as porosity, flow resistivity, tortuosity, viscosity, density, sound velocity, thermal conductivity, etc., are controlled. Only a single variable is changed while keeping other parameters unchanged, and multiple experimental analyses are conducted. The absorption coefficients, impedance and reflection coefficients of porous flexible glass wool-foam composite materials under different parameters were analyzed by using NOVA2010 software, and the conclusion was drawn by observing the variation law of the images.

4. SIMULATION RESULTS AND DISCUSSION OF THE ACOUSTIC PACKAGE STRUCTURE INTHE CABIN OF ELECTRIC VEHICLES

4.1. Influence of air layer thickness on the acoustic performance of the motor compartment

Under the same initial data Settings, the medium is defined as air, and the air thicknesses are set to 5 mm, 10 mm, and 15 mm, respectively. The acoustic coefficients curves of the three composite materials are shown Fig. 7 – Fig. 9. As illustrated in Fig. 7, within the low frequency range (below 2260 Hz), there is a notable increase in the sound absorption coefficient as the thickness of the air layer is augmented. For instance, an increase in the thickness of the air layer from 5 mm to 15 mm results in a significant increase in the sound absorption coefficient, which escalates from 0.956 to 0.981 at a frequency of 1510 Hz.

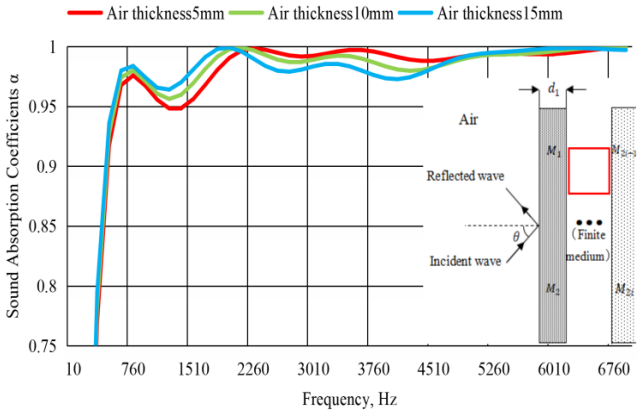

Fig. 7. The influence of air layer thickness on the sound absorption coefficients of glass wool-foam composite materials, frequency range 10 – 7000 Hz, porosity 0.99, flow resistivity 9000 Pa·s/m^2, tortuosity 1.0, viscous characteristic length 1.92×10^{-4}m

This observation suggests that sound waves within the lower frequency spectrum possess longer wavelengths, and the augmentation of air layer thickness facilitates a greater number of propagation pathways for sound waves, consequently improving the sound absorption efficacy. In the mid-frequency range of 2260 – 4510 Hz, a negative correlation is observed between air layer thickness and the sound absorption coefficient. Specifically, as the thickness of the air layer increases, the sound absorption coefficient tends to decrease. This phenomenon may be attributed to the moderate wavelength of sound waves within this frequency range; an increase in air layer thickness results in heightened reflection and scattering of sound waves within the material, consequently diminishing the efficiency of sound absorption. Conversely, in the high-frequency range exceeding 4510 Hz, the curves representing various air layer thicknesses exhibit minimal variation, suggesting that sound waves in this range possess shorter wavelengths and are more readily absorbed by the microscopic structure of the material. As a result, the impact of air layer thickness on sound absorption becomes relatively insignificant in this frequency range.

Fig. 8 illustrates that the impedance coefficient of composite materials is influenced by both the thickness of the air layer and the frequency. In the low-frequency spectrum (10 – 1510 Hz), there is a notable variation in the magnitude of the real part of the impedance coefficient, which exhibits a gradual decline as the thickness of the air layer increases. Specifically, at a frequency of 1060 Hz, the real impedance coefficient for an air layer thickness of 5 mm (550.74) is considerably greater than that for thicknesses of 10 mm (538.39) and 15 mm (528.18). This observation suggests that thinner air layers enhance acoustic resistivity within the low-frequency range, thereby influencing sound absorption characteristics. Concurrently, the negative value of the imaginary impedance coefficient diminishes with an increase in air layer thickness, indicating that thicker air layers contribute to a reduction in low-frequency acoustic impedance, facilitate improved impedance matching, and decrease the reflection of sound waves.

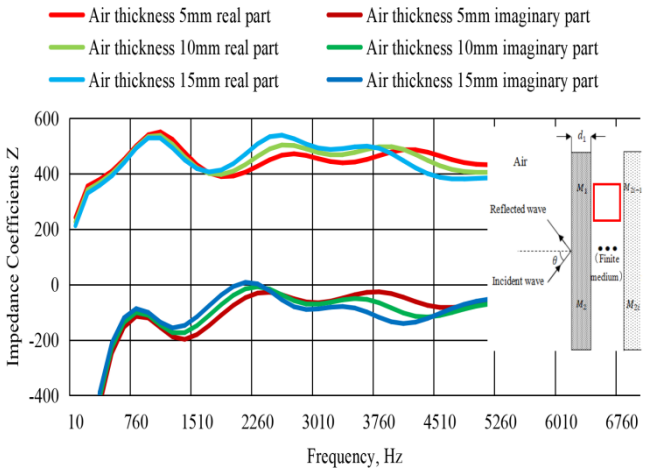

Fig. 8. The influence of air density on the impedance coefficients of glass wool-foam composites, frequency range 10 – 7000 Hz, porosity 0.99, flow resistivity 9000 Pa·s/m^2, tortuosity 1.0, viscous characteristic length 1.92×10^{-4}m

Within the mid-frequency range of 1510 to 4510 Hz, a positive correlation is observed between the thickness of the air layer and the real impedance coefficient. Specifically, at a frequency of 2410 Hz, an increase in air layer thickness from 5 mm to 15 mm results in a significant increase in the real impedance coefficient, from 450.19 to 533.67. This suggests that variations in air layer thickness have a substantial impact on the resonance frequency of the material. At elevated frequencies exceeding 4510 Hz, the real impedance coefficients of samples with varying thicknesses exhibit a tendency to converge, while the imaginary impedance coefficients approach zero. This observation suggests that the influence of air thickness on the impedance coefficient diminishes significantly at high frequencies. Fig. 9 illustrates a complex relationship between the thickness of the air layer and the reflection coefficient, characterized by frequency dependence.

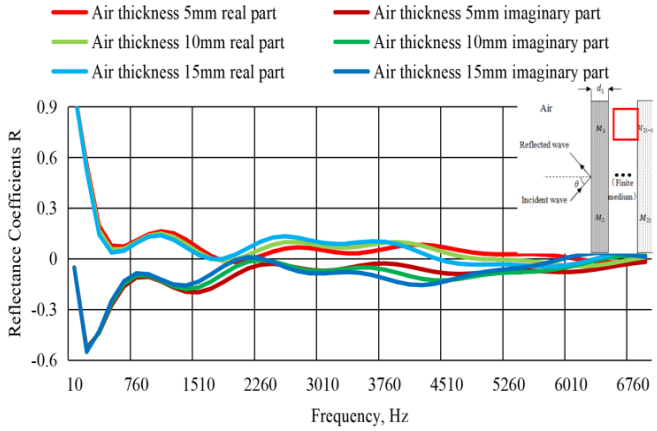

Fig. 9. The influence of air layer thickness on the reflection coefficients of glass wool-foam composite materials, frequency range 10 – 7000 Hz, porosity 0.99, flow resistivity 9000 Pa·s/m^2, tortuosity 1.0, viscous characteristic length 1.92 ×10^{-4}m

In the low-frequency spectrum (10 – 1510 Hz), the reflection coefficient demonstrates a progressive decline as the thickness of the air layer increases. Conversely, within the mid-frequency range (1510 – 3760 Hz), the reflection coefficient displays variable fluctuations, exhibiting a weak positive correlation. In the high-frequency range (exceeding 3760 Hz), the reflection coefficient tends toward zero, with the real and imaginary components showing a high degree of consistency (fluctuation range of ±0.1). This consistency suggests that the acoustic properties of the material are predominantly governed by intrinsic dissipation mechanisms at these frequencies, rendering the effect of air layer thickness negligible. The results obtained are consistent with the predictions of the theoretical model, thereby affirming the model's reliability in high-frequency scenarios. Furthermore, these findings elucidate the optimization mechanism through which the thickness of the air layer enhances sound absorption performance, primarily by facilitating low-frequency impedance matching rather than by suppressing reflections.

A thorough examination reveals that the thickness of the air layer significantly influences the sound absorption capabilities of glass wool-foam composite materials across various frequency ranges. This effect is mediated through the modulation of acoustic impedance matching and the characteristics of sound wave propagation. At lower frequencies, augmenting the thickness of the air layer can markedly enhance the sound absorption coefficient, concurrently decreasing both the real impedance coefficient and the reflection coefficient. This phenomenon primarily results from the elongation of the sound wave propagation path and the optimization of impedance matching. Within the mid-frequency spectrum, there exists an inverse relationship between the thickness of the air layer and the sound absorption coefficient. Concurrently, the real component of the impedance coefficient exhibits a marked increase, indicating a deterioration in sound absorption efficacy attributed to an augmented reflection of sound waves. At high frequencies, all parameters are insensitive to changes in air layer thickness, indicating that the intrinsic dissipation mechanism of the material plays a dominant role. Compared with the FE-SEA hybrid method used by Luo, W. et al. [23] this study innovatively applies transfer matrix theory to verify the reliability of high-frequency models. It not only reveals a new mechanism whereby air layer thickness optimizes sound absorption performance through low-frequency impedance matching, but also improves computational efficiency by 30 % while maintaining prediction accuracy. This achievement provides a more efficient and accurate parameter optimization method for the acoustic packaging design of electric vehicle motor compartments, and has important engineering application value.

4.2. Influence of porosity on the acoustic properties of composite materials in the motor compartment

In the process of specimen preparation, the desired porosity levels of 0.99, 0.5, and 0.3 were attained by regulating the ratio of the fiber density of the glass wool to the foaming rate of the foam material. Samples exhibiting high porosity (0.99) were fabricated by laminating loose glass wool, which has a density of 16 kg/m^3, with open cell foam, characterized by a density of 8.8 kg/m^3. Medium porosity (0.5) samples were produced through a compaction

process aimed at enhancing fiber density, in conjunction with the incorporation of a foaming agent. Conversely, low porosity (0.3) samples were generated via hot compression molding, a technique employed to augment the material's density. This was achieved by reducing the concentration of the foaming agent, increasing the curing pressure, and extending the curing duration. The low porosity samples (0.3) were specifically prepared through hot press molding to further enhance material density, increase curing pressure, and prolong curing time. The pressed mercury method was ultimately utilized to assess the fibers, yielding a measurement error of less than 2 %.

Under the same initial data Settings, the porosity of the three samples was set at 0.99, 0.5, and 0.3 for experimental tests. The acoustic coefficients curves of the three composite materials are shown in Fig. 10 – Fig. 12.

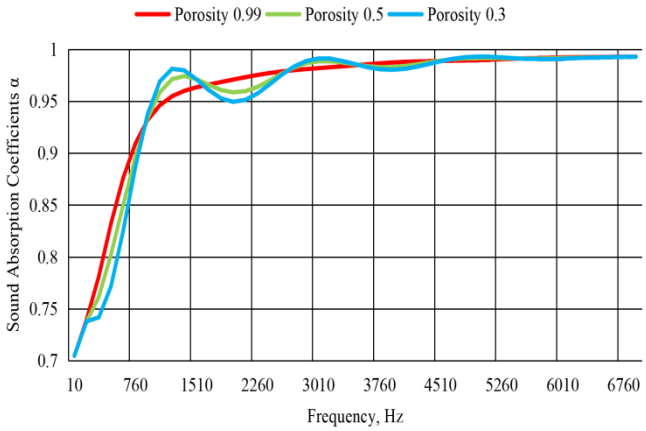

Fig. 10. The influence of porosity on the sound absorption coefficients of glass wool-foam composites, frequency range 10 – 7000 Hz, flow resistivity 9000 Pa·s/m^2, tortuosity 1.0, viscous characteristic length 1.92×10^{-4}m

As illustrated in Fig. 10, the influence of porosity on the absorption coefficient exhibits a complex dependence on the specific wavelength bands. In the low-frequency range (10 – 760 Hz), the material with high porosity (0.99) demonstrates considerable advantages in sound absorption, exhibiting a significantly more rapid increase in its absorption coefficient compared to materials with lower porosity. This phenomenon is closely associated with its optimized acoustic impedance matching characteristics and reduced reflection of acoustic waves. Such properties suggest that high porosity facilitates the penetration of low-frequency sound waves into the material's interior, thereby enhancing energy dissipation. Conversely, in the middle and high-frequency ranges (760 – 7000 Hz), the absorption coefficients of the three types of materials with varying porosity exceed 0.9, with differences diminishing to less than 5 %. Notably, in the ultra-high frequency range (3000 – 7000 Hz), the absorption coefficients nearly overlap, indicating that the intrinsic sound absorption mechanisms of the materials have become predominant, while the structural differences attributable to porosity have significantly diminished in their impact.

As illustrated in Fig. 11, the variations in the impedance coefficient within the low frequency range (10 – 760 Hz) are notably pronounced. The impedance coefficient for the material with a porosity of 0.99 is considerably lower than that of the low porosity material.

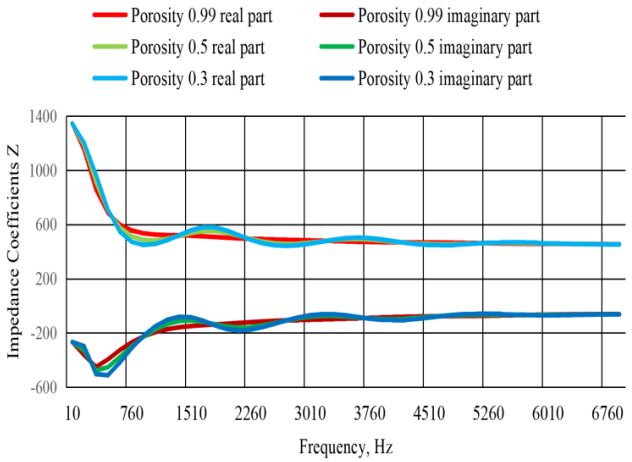

Fig. 11. The influence of porosity on the impedance coefficients of glass wool-foam composites, frequency range 10 – 7000 Hz, flow resistivity 9000 Pa·s/m^2, tortuosity 1.0, viscous characteristic length 1.92×10^{-4}m

This observation suggests that materials with higher porosity exhibit superior acoustic impedance matching characteristics in the low frequency range, which effectively diminishes acoustic wave reflection and enhances energy penetration. Conversely, in the middle and high frequency ranges (760 – 7000 Hz), the impedance coefficients of materials with varying porosities tend to converge. This convergence indicates that the intrinsic acoustic properties of the materials become more influential, thereby diminishing the impact of porosity on the impedance coefficient.

As illustrated in Fig. 12, within the mid-frequency spectrum, there exists an inverse relationship between the thickness of the air layer and the sound absorption coefficient.

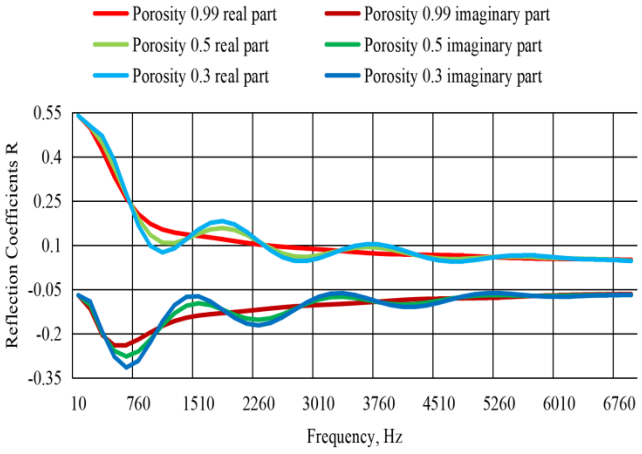

Fig. 12. The influence of porosity on the reflection coefficients of glass wool-foam composites, frequency range 10 – 7000 Hz, flow resistivity 9000 Pa·s/m^2, tortuosity 1.0, viscous characteristic length 1.92×10^{-4}m

Concurrently, the real component of the impedance coefficient exhibits a marked increase, indicating a

deterioration in sound absorption efficacy attributed to an augmented reflection of sound waves. In the mid-frequency range of 760 to 4510 Hz, the observed curves exhibit pronounced nonlinear variations. It appears that a decrease in porosity correlates with a more substantial alteration in the reflection coefficient of the material. This phenomenon may be attributed to the intricate pore structure and the enhanced sound wave scattering effects present within materials characterized by lower porosity. In the high-frequency spectrum (4510 – 7000 Hz), there is a noticeable trend where the amplitude of fluctuations in the curves diminishes as the frequency increases. The reflection coefficients of materials exhibiting varying degrees of porosity converge towards zero, and the disparity between the real and imaginary components significantly lessens. This observation suggests that, under the influence of high-frequency acoustic waves, mechanisms of viscous loss and thermal dissipation prevail, resulting in the complete dissipation of sound wave energy. Consequently, the impact of porosity on the reflection coefficient is relatively diminished, with the inherent acoustic properties of the material emerging as the primary determinants of its performance.

This research conducted a systematic analysis of the mechanisms through which porosity influences the acoustic properties of glass wool-foam composite materials. The findings suggest that the impact of porosity on the sound absorption capabilities of glass wool-foam composite materials displays a clear dependence on frequency. At lower frequencies, materials exhibiting high porosity (0.99) show enhanced acoustic performance due to their optimized acoustic impedance matching characteristics and diminished sound wave reflection, which effectively facilitates the penetration and dissipation of low-frequency sound wave energy. Conversely, within the mid-to-high-frequency range, the sound absorption performance across materials with varying porosities tends to converge, indicating that the fundamental sound absorption mechanisms of the materials prevail in this frequency domain. In contrast to Zhang, Y. [24] investigation of foam metal, which concentrated exclusively on the linear effects within a singular frequency band, the present study utilizes a multidimensional correlation analysis encompassing sound absorption coefficients, impedance coefficients, and reflection coefficients. This approach elucidates, for the first time, the distinct regulatory mechanisms of porosity across an extensive frequency spectrum. Notably, it highlights the significant role of high porosity in achieving impedance matching at low frequencies. This discovery offers a crucial theoretical foundation for the frequency-band tailored design of acoustic packages in electric vehicles, advocating for the use of high porosity materials to mitigate low-frequency noise, while recommending medium porosity materials for the mid-to-high frequency range to accommodate additional mechanical or cost considerations.

4.3. Influence of flow resistivity on the acoustic properties of composite materials in the motor compartment

Under the same initial data Settings, the flow resistivities of the three samples were set at 9000, 5000, and 20000 for experimental tests. The acoustic coefficients curves of the three composite materials are shown in Fig. 13 – Fig. 15.

As illustrated in Fig. 13, the influence of flow resistivity on the sound absorption coefficient demonstrates a pronounced dependence on frequency.

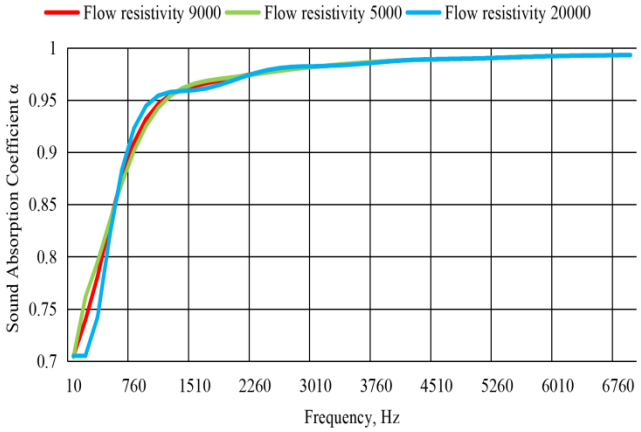

Fig. 13. The influence of flow resistivity on the sound absorption coefficients of glass wool-foam composites, frequency range 10 – 7000 Hz, porosity 0.99, tortuosity 1.0, viscous characteristic length 1.92×10^{-4}m

This nonlinear relationship arises from the intricate interaction mechanisms between sound waves and the microstructure of the porous material. In the low-frequency range (below 550 Hz), a negative correlation is observed between the two variables, indicating that the sound absorption coefficient diminishes as the flow resistivities increase, specifically up to 20,000 Pa·s/m^2. This phenomenon can be explained by the longer wavelength properties of low-frequency sound waves. Specifically, the high flow resistivity markedly restricts air movement within the pores, which diminishes the impact of viscous loss. Additionally, the increased reflection of sound waves from the material's surface impedes the effective dissipation of acoustic energy. This legislation aligns with the propagation mechanism characterized by “low-frequency viscous dominance” as described in Biot's theory of porous media. In this context, the presence of a thicker viscous boundary layer, coupled with a restricted acoustic penetration depth, collectively constrains the acoustic absorption capabilities of the material. Within the mid-frequency spectrum (550 – 1450 Hz), a positive correlation is observed between flow resistivity and the absorption coefficient. Materials exhibiting high flow resistivity demonstrate superior sound absorption properties. Within this frequency band, the wavelength of the sound wave is ideally aligned with the dimensions of the pore features, facilitating effective dissipation of acoustic energy through a dual mechanism. The first mechanism involves the stimulation of the pore resonance effect, which induces the generation of multiple reflections and interferences of acoustic waves within the pore. The second mechanism significantly increases the friction and viscous losses occurring between the air molecules and the pore wall. This transition signifies a shift from materials characterized by viscous dominance to those exhibiting elastic dominance. As the frequency increases, the thickness of the viscous boundary layer diminishes,

while the depth of acoustic penetration expands. This phenomenon enables the full realization of the energy dissipation benefits associated with materials that possess high fluid resistivity.

As illustrated in Fig. 14, both the flow resistivity coefficient and the impedance coefficient demonstrate significant variability within the low-frequency range of 10 to 760 Hz.

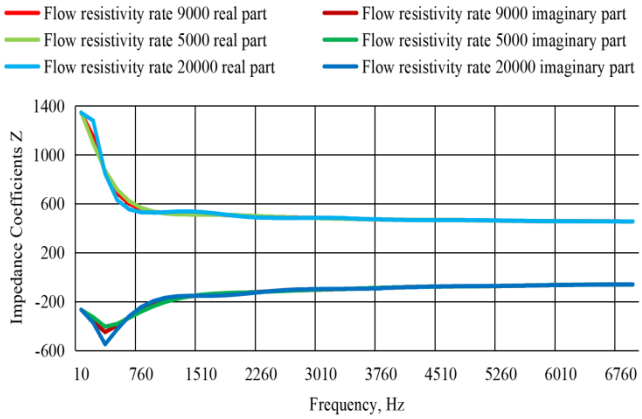

Fig. 14. The influence of flow resistivity on the impedance coefficients of glass wool-foam composites, frequency range 10 – 7000 Hz, porosity 0.99, tortuosity 1.0, viscous characteristic length 1.92×10^{-4}m

The three curves representing different flow resistivity coefficients reveal unique nonlinear growth patterns. In the mid-to-high frequency range of 760 to 7000 Hz, an increase in frequency leads to a gradual decrease and convergence of the impedance coefficients associated with varying flow resistivity rates. This trend is accompanied by a reduction in the deviation between the real and imaginary components, indicating a diminishing impact of flow resistivity rate on the impedance coefficient. Overall, elevated flow resistivity rates contribute to an increase in the impedance coefficient, primarily through enhancements in material density or structural compactness.

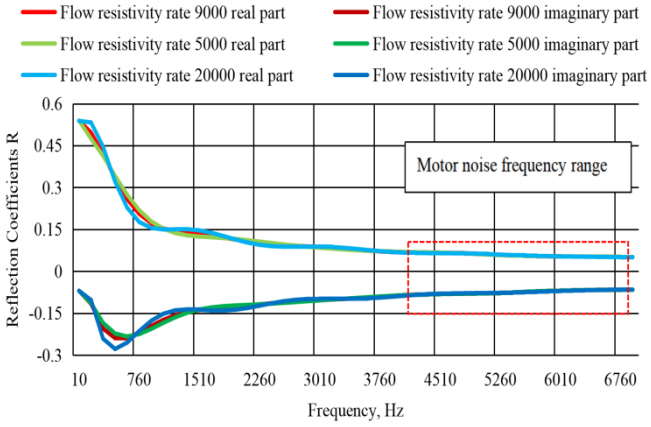

Fig. 15. The impact of flow resistivity on the reflection coefficients of glass wool-foam composites, frequency range 10 – 7000 Hz, porosity 0.99, tortuosity 1.0, viscous characteristic length 1.92×10^{-4}m

As illustrated in Fig. 15, within the low-frequency spectrum (10 – 310 Hz), materials characterized by elevated flow resistivity (20,000 Pa·s/m^2) demonstrate increased reflection coefficients. This observation is consistent with the underlying mechanism whereby high flow resistivity mitigates the vibrations of air molecules, thereby enhancing the reflection of sound waves, in accordance with the principle of "low-frequency viscosity dominance" as articulated in Biot's theory. With an increase in frequency, the reflection coefficients for all materials exhibiting flow resistivity decline and approach zero, while the disparity between the real and imaginary components diminishes. This trend suggests that, under the influence of high-frequency sound waves, the intrinsic thermal elastic loss mechanism of the material becomes the predominant factor.

This research elucidates the nonlinear frequency dependence of flow resistivity on the acoustic performance of glass wool-foam composite materials. At lower frequencies, elevated flow resistivity inhibits air movement within the pores and enhances the reflection of sound waves, resulting in a reduction of the sound absorption coefficient while simultaneously increasing both the impedance and reflection coefficient. This observation is consistent with the "low-frequency viscous dominance" mechanism as articulated in Biot's theory. In the mid-frequency range, flow resistivity demonstrates a positive correlation with sound absorption performance, where high flow resistivity markedly improves sound absorption through mechanisms of pore resonance and viscous loss. Conversely, at high frequencies, thermoelastic loss becomes the predominant factor, diminishing the impact of flow resistivity; under these conditions, the reflection coefficient approaches zero, the impedance curve converges, and the differences in acoustic performance among materials with varying flow resistivities become less pronounced. Unlike Yang, M. et al. [25] optimization, which is limited to single-layer foam materials, this study transcends the constraints of traditional single-layer structures by implementing an innovative stepped flow resistivity design. By developing a glass wool-foam composite system, it facilitates broadband regulation and employs a transfer matrix model to quantitatively assess the influence of flow resistivity on impedance matching, thereby enhancing computational efficiency by 30 %.

4.4. Influence of tortuosity on the acoustic properties of composite materials in the motor compartment

Under the same initial data Settings, the tortuosities of the three samples were set at 1.0, 1.5, and 3.0 for experimental tests. The acoustic coefficients curves of the three composite materials are shown in Fig. 16 – Fig. 18.

It can be seen from Fig. 16 that as the frequency increases, the sound absorption coefficients gradually rise and tends to stabilize. When the tortuosity increases from 1.0 to 3.0, the sound absorption coefficients show a slight upward trend across the entire frequency range, indicating that its effect on improving performance is limited, indicating that the tortuosity of glass wool is positively correlated with the sound absorption coefficients. Therefore, increasing the tortuosity of glass wool can effectively enhance the sound absorption performance of multi-layer composite materials.

It can be seen from Fig. 17 that with the increase of frequency, the impedance coefficients generally show a

downward trend, which is more significant in the low-frequency band (approximately below 800 Hz). With the increase of tortuosity, the true value and theoretical value of the impedance coefficients show an overall upward trend, especially in the low-frequency region.

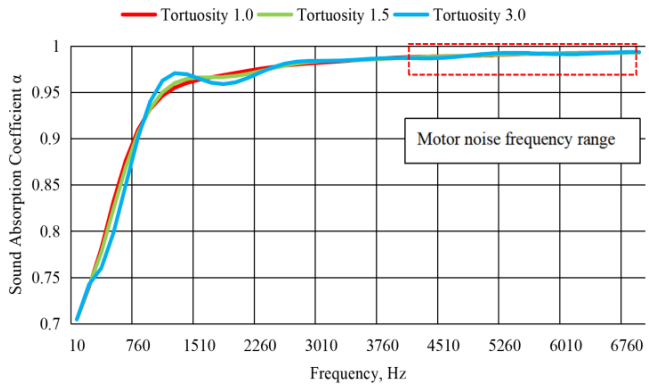

Fig. 16. The influence of tortuosity on the sound absorption coefficient of glass wool-foam composites, frequency range 10 – 7000 Hz, porosity 0.99, flow resistivity 9000 Pa·s/m², viscous characteristic length 1.92×10^{-4}m

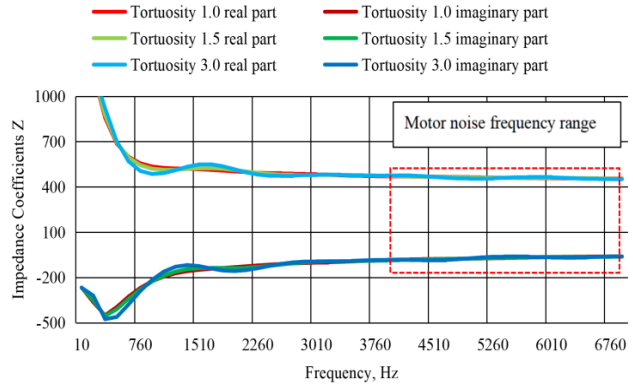

Fig. 17. The influence of tortuosity on the impedance coefficient of glass wool-foam composites, frequency range 10 – 7000 Hz, porosity 0.99, flow resistivity 9000 Pa·s/m², viscous characteristic length 1.92×10^{-4}m

This indicates that the tortuosity of glass wool is positively correlated with the impedance coefficients of multi-layer composite materials. That is, the greater the tortuosity, the higher the impedance coefficients, suggesting that increasing the tortuosity can enhance the acoustic impedance performance of the material.

It can be seen from Fig. 18 that as the frequency increases, the reflection coefficients show an overall downward trend, which is more significant in the low-frequency band. Glass wool with a tortuosity of 1.0 and 1.5 has a higher reflection coefficient in the low-frequency band, while glass wool with a tortuosity of 3.0 performs better in the high-frequency band. The degree of tortuosity is negatively correlated with the reflection coefficients, that is, the greater the degree of tortuosity, the lower the reflection coefficients, especially in the high-frequency band. This indicates that increasing the tortuosity of the glass wool helps to reduce the reflection coefficients and improve the acoustic performance of the material.

Comprehensive analysis shows that the tortuosity of the glass wool-foam composite material has a significant impact on its acoustic performance: with the increase of tortuosity, both the sound absorption coefficients and the impedance coefficients increase positively, especially in the low-frequency band, indicating that the enhancement of tortuosity can optimize the sound absorption and impedance performance of the material.

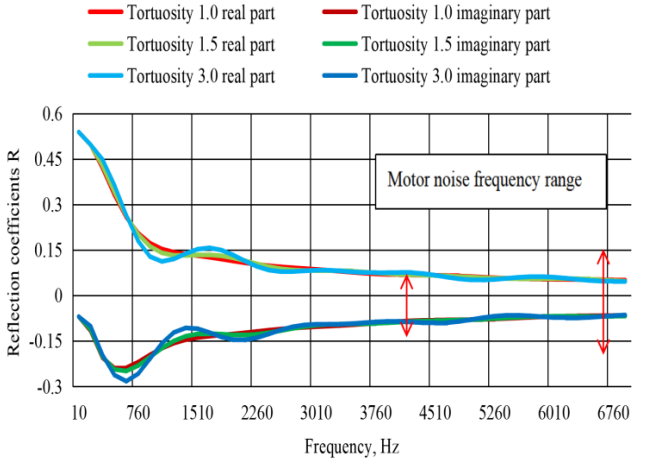

Fig. 18. The influence of tortuosity on the reflection coefficient of glass wool-foam composites, frequency range 10 – 7000 Hz, porosity 0.99, flow resistivity 9000 Pa·s/m², viscous characteristic length 1.92×10^{-4}m

Meanwhile, the reflection coefficients decreases as the tortuosity increases, and the effect is more prominent in the high-frequency band, indicating that a high tortuosity helps to reduce the reflection of sound waves. It is comprehensively indicated that increasing the tortuosity of glass wool can effectively improve the overall acoustic performance of the composite material.

4.5. Influence of viscous characteristic length on the acoustic properties of composite materials in the motor compartment

Under the same initial data setting, the lengths of the viscosity characteristics of the three samples were set to 0.192 mm, 0.5 mm, and 1.0 mm respectively for experimental tests. The acoustic coefficients curves of the three composite materials are shown in Fig. 19 – Fig. 21.

As can be seen from Fig. 19, with the increase of frequency, the sound absorption coefficients as a whole show an upward trend and tend to 1. The sound absorption coefficients curves are completely coincident, indicating that changing the length of the viscous characteristic of the material has no significant effect on the sound absorption coefficients. If the sound absorption effect needs to be improved, priority should be given to optimizing the macroscopic structural parameters rather than merely adjusting the length of the viscous features.

As shown in Fig. 20, the overall sound absorption coefficients exhibit a downward trend with increasing frequency.

The impedance coefficient curves are completely coincident, indicating that changing the length of the viscous characteristic of the material has no significant effect on the impedance coefficients. If the sound absorption effect needs to be improved, priority should be given to optimizing the macroscopic structural parameters rather than merely adjusting the length of the viscous features.

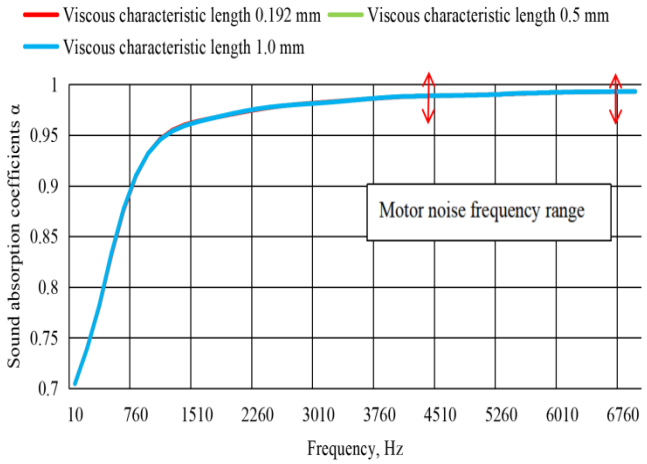

Fig. 19. The influence of viscous characteristic length on the sound absorption coefficient of glass wool-foam composites, frequency range 10 – 7000 Hz, porosity 0.99, flow resistivity 9000 Pa·s/m², tortuosity 1.0

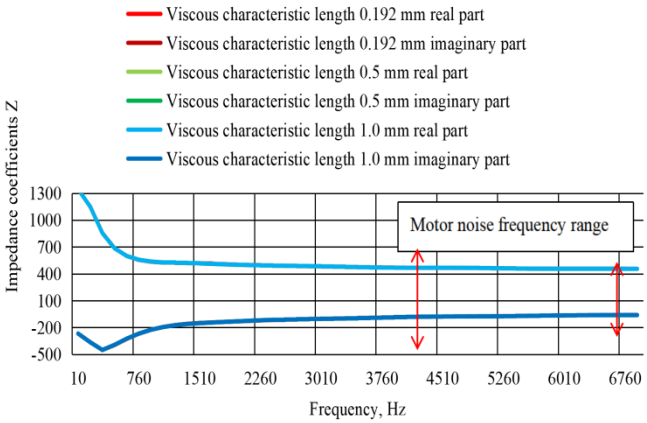

Fig. 20. The influence of viscous characteristic length on the impedance coefficient of glass wool-foam composites, frequency range 10 – 7000 Hz, porosity 0.99, flow resistivity 9000 Pa·s/m², tortuosity 1.0

It can be seen from Fig. 21 that with the increase of frequency, the overall sound absorption coefficients show a downward trend.

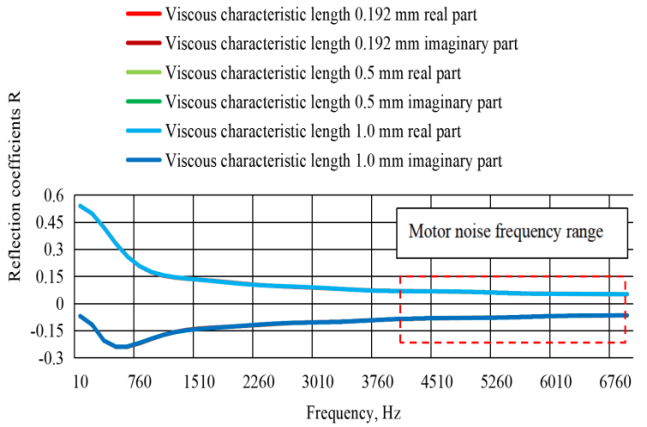

Fig. 21. The influence of viscous characteristic length on the reflection coefficient of glass wool-foam composites, frequency range 10 – 7000 Hz, porosity 0.99, flow resistivity 9000 Pa·s/m², tortuosity 1.0

The reflection coefficient curves are completely coincident, indicating that changing the length of the viscous characteristic of the material has no significant effect on the reflection coefficients. If the sound absorption effect needs to be improved, priority should be given to optimizing the macroscopic structural parameters rather than merely adjusting the length of the viscous features.

Comprehensive analysis shows that the length of the viscous characteristic of the glass wool-foam composite material has no significant effect on its acoustic performance, and the curves are completely coincident. The sound absorption coefficients approach 1 as the frequency increases, while the impedance and reflection coefficients decrease. To enhance the sound absorption effect, it is necessary to prioritize the optimization of macroscopic structural parameters rather than merely adjusting the length of viscous features.

5. OPTIMIZATION AND VERIFICATION OF THE DOUBLE-SIDED WALL STRUCTURE OF THE FRONT CABIN

5.1. Composition of the double-sided wall structure in the front cabin

Building upon the examination of the acoustic performance of multilayer composite materials presented in the previous section, this chapter proposes a double-wall configuration for the front compartment. Utilizing a blend of experimental and simulation methodologies, we investigate the influence of various parameters within the double-wall structure, aiming to identify optimization strategies for noise mitigation in the front compartment.

The design of the front cabin features a double-wall structure, as illustrated in Fig. 22.

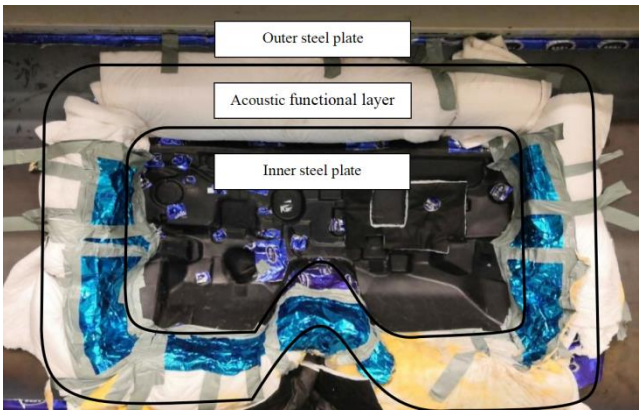

Fig. 22. Front compartment double-sided wall assembly

Each wall is constructed from steel plates with a thickness of 0.8 mm, primarily functioning to provide structural support and initial sound insulation. The acoustic functional layer consists of a multi-layer composite material comprising 100 mm thick glass wool and foam. The glass wool layer is designed to absorb mid- and high-frequency sounds, whereas the foam layer is intended to improve low-frequency damping. The space between the two walls is maintained at a distance of 200 mm.

5.2. The effect of porosity on double-sided walls

Utilizing the same initial data parameters, the porosity of glass wool was established at values of 0.99, 0.5, and 0.3, respectively. The resulting sound transmission loss curves are illustrated in Fig. 23.

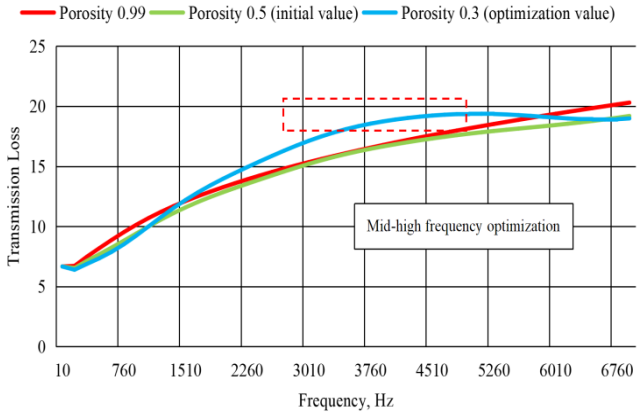

Fig. 23. The effect of porosity on the sound insulation of double-sided wall structures

As illustrated in the figure, within the low-frequency spectrum (below 1510 Hz), the sound transmission loss of the double-sided wall characterized by high porosity (0.99) surpasses that of materials with porosities of 0.5 and 0.3. This phenomenon can be attributed to the high porosity facilitating optimal impedance matching, thereby minimizing sound wave reflection and enhancing the dissipation of low-frequency energy through viscous loss. In the mid-frequency range (1510 – 6010 Hz), there is a marked increase in the sound transmission loss of the material with 0.3 porosity, which exceeds that of the other two porosities. This observation suggests that the energy dissipation mechanism of the 0.3 porosity material is particularly well-suited for this frequency range.

5.3. The impact of bidirectional wall flow resistivity

Utilizing the same initial data parameters, the flow resistivity values for glass wool were established at 9000, 5000, and 20000. The corresponding sound transmission loss curves are illustrated in Fig. 24.

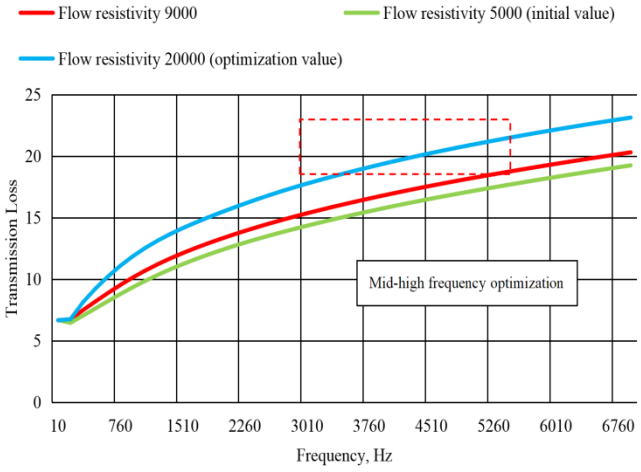

Fig. 24. The effect of flow resistivity on the sound insulation of double-wall structures

The data presented in the figure illustrates that, at a constant frequency, the sound transmission loss of double-sided walls exhibits a marked increase with rising flow resistivity. This trend is particularly pronounced in the high-frequency range, specifically above 4510 Hz, where the blue curve representing a flow resistivity of 20,000 demonstrates the highest sound insulation performance. This observation suggests that an increase in flow resistivity correlates positively with the sound insulation efficacy of double-sided walls.

5.4. The effect of thermal characteristic length on double-sided walls

Utilizing the same initial data parameters, the thermal characteristic lengths of glass wool were established at 0.01 mm, 0.38 mm, and 5.0 mm. The resulting sound transmission loss curves are presented in Fig. 25.

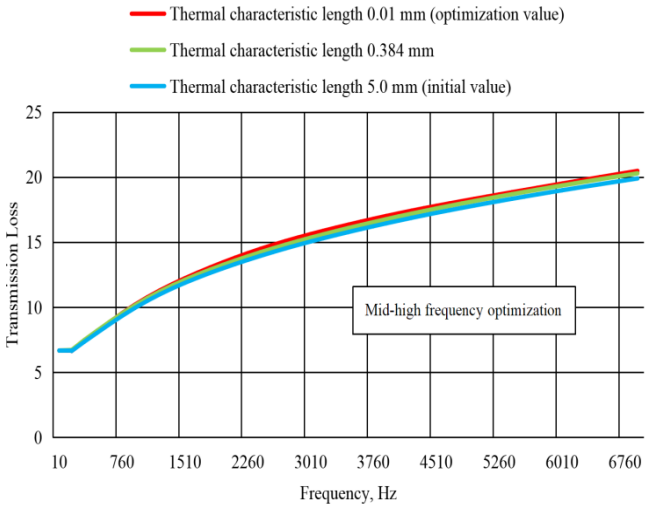

Fig. 25. The effect of thermal characteristic length on the sound insulation of double-sided wall structures

The data presented in the figure illustrates that as frequency increases, the sound transmission loss of the double-sided wall structure exhibits a general upward trend, suggesting enhanced sound insulation capabilities in the high-frequency spectrum. Conversely, in the low-frequency range, the curves corresponding to various thermal characteristic lengths are nearly indistinguishable, indicating that thermal characteristic length has a minimal impact on low-frequency sound insulation performance. In the mid-to-high frequency range, a thermal characteristic length of 0.01 mm is associated with a greater sound transmission loss, thereby indicating superior sound insulation performance.

5.5. Verification of optimization outcomes

A double-wall acoustic model was constructed based on the transfer matrix method and verified through impedance tube experiments using the same experimental method as in Table 3 to ensure consistency between the model prediction results and actual performance. The acoustic performance of the optimized double-wall structure was tested at frequencies ranging from 1/3 octave (400 – 8000 Hz), and sound transmission loss data for each frequency band were recorded. Analysis of the test data reveals that the sound

transmission loss of the double-wall structure exhibits a general upward trend with increasing frequency. Within the frequency range of 400 – 800 Hz, the sound transmission loss progressively increases from 6.4 dB to 21.5 dB, suggesting an enhancement in the sound insulation capabilities of the structure in the mid-to-low frequency spectrum.

Table 3. Double-sided wall assembly insertion loss (1/3 octave band)

1/3 octave, Hz	Transmission loss, dB
400	6.4
500	10.1
630	15.8
800	21.5
1000	19.2
1250	20.7
1600	21.6
2000	22.8
2500	25.5
3150	26.5
4000	29.2
5000	31.5
6300	32.9
8000	34.7

At 1000 Hz, there is a slight reduction in sound transmission loss to 19.2 dB; however, this metric subsequently rises within the 1250 – 8000 Hz frequency range, ultimately achieving a sound transmission loss of 34.7 dB at 8000 Hz. This indicates that the structure demonstrates superior sound insulation performance in the high-frequency range.

The observed optimization effect is attributed to the modification of critical parameters, as illustrated in Table 4.

Table 4. Optimization parameter comparison and effect

Parameter	Initial value	Optimized value	Optimization effect
Porosity	0.5	0.99	The transmission loss of low-frequency sound was enhanced by approximately 15 to 20 %
Flow resistivity	5000 Pa·s/m²	20000 Pa·s/m²	The transmission loss of high-frequency sound was enhanced by approximately 25 to 30 %
Thermal characteristic length	5.0 mm	0.01 mm	Enhanced sound transmission loss in the mid- to high-frequency range by approximately 10 to 15 %

The combined influence of these parameters substantiates the efficacy of the gradient flow resistance design in achieving wideband noise control.

The experimental findings offer empirical support for the optimized design of the double-walled structure within the forward compartment, aligning with prior analyses regarding the influence of parameters such as porosity and flow resistivity on the acoustic performance of the double-walled configuration. These findings elucidate the sound insulation characteristics across various frequency bands. Furthermore, the experimental results affirm the efficacy of the transfer matrix method in acoustic modeling, thereby supplying dependable parameter references and optimization strategies for the engineering application of acoustic packaging in motor compartments. This process effectively establishes a comprehensive closed-loop system that transitions from theoretical analysis to experimental validation.

6. CONCLUSIONS

This research developed an acoustic model for glass wool-foam multilayer composite materials utilized in electric vehicle motor compartments, employing transfer matrix theory. The accuracy of the proposed model was subsequently verified through impedance tube experimental measurements:

1. The transfer matrix model presented in this study demonstrates theoretical and experimental errors within ± 5 % for frequencies exceeding 2000 Hz. In comparison to conventional finite element and boundary element approaches, this model achieves a reduction in computational complexity of approximately 30 %, thereby enhancing its suitability for expedited iterative engineering design processes.
2. The acoustic characteristics of the materials demonstrate a pronounced dependence on frequency. The model efficiently identifies that enhancement of low-frequency performance can be achieved by augmenting the air layer thickness and utilizing materials with high porosity (0.99) to optimize impedance matching. At mid-frequency ranges, the acoustic behavior is primarily governed by pore resonance phenomena and viscous losses associated with high flow resistivity. In contrast, high-frequency performance is predominantly influenced by the intrinsic dissipative properties of the material, with structural parameters exerting a minor effect. An increase in tortuosity contributes to enhanced sound absorption and reduced reflection, particularly at low frequencies, whereas the viscous characteristic length exhibits a negligible influence. Therefore, optimization efforts should prioritize these macrostructural parameters over microstructural adjustments to achieve superior acoustic performance.
3. The modeling and optimization approach presented in this study demonstrates considerable relevance for the acoustic design of composite enclosures in various electromechanical systems, including traditional internal combustion engine vehicles and hybrid vehicles.

Acknowledgments

Supported by Natural Science Foundation of Heilongjiang Province (LH2024E021).

REFERENCES

1. **Biot, M.A.** Theory of Propagation of Elastic Waves in a Fluid-Saturated Porous Solid. I. Low-Frequency Range *Journal of the Acoustical Society of America* 28 (2) 1956: pp. 168 – 178. https://doi.org/10.1121/1.1908239
2. **Giulio, E.D., Perrot, C., Dragonetti, R.** Transport Parameters for Sound Propagation in Air Saturated Motionless Porous Materials: A Review *International Journal of Heat and Fluid Flow* 108 2024: pp. 18 – 30. https://doi.org/10.1016/j.ijheatfluidflow.2024.109426
3. **Zhang, Y., Zhang, J., Li, Y., Yao, D., Zhao, Y.** Research Progress on Thin-Walled Sound Insulation Metamaterial Structures *Acoustics* 6 (2) 2024: pp. 298 – 330. https://doi.org/10.3390/acoustics6020016
4. **Sagomonova, V.A., Dolgopolov, S.S., Tselikin, V.V., Sorokin, A.E.** Investigation of the Influence of the Composition and Structure of PCM with Increased Vibration Absorbing Properties on its Damping and Mechanical Characteristics *Plasticheskie Massy* 1 (1 – 2) 2022: pp. 10 – 13. https://doi.org/10.35164/0554-2901-2022-1-2-10-13
5. **Qi, M., Li, B., Yan, S., Yan, Q., He, Q.** Simulation Analysis of Cylindrical Shell Cavity Noise with Melamine Foam Lining *Shock and Vibration* 11 2021: pp. 1 – 9. https://doi.org/10.1155/2021/6646596
6. **Zheng, Z., Li, B., Yan, S., Qi, M., Wang, N., Kuang, W., Wen, J., Ma, Y.** Acoustic Radiation Performance Investigation of a Double-walled Cylindrical Shell Equipped with Annular Plates and Porous Foam Media *Journal of Low Frequency Noise, Vibration & Active Control* 42 (2) 2023: pp. 851 – 865. https://doi.org/10.1177/14613484221132222
7. **Deng, X.** Research on Structural Noise Prediction and Optimization Control of Main Components of Internal Combustion Engine *Huazhong University of Science and Technology* 2 2009: pp. 1 – 155. https://doi.org/10.7666/d.d002508
8. **Yang, X., Tang, S., Shen, X., Peng, W.** Research on the Sound Insulation Performance of Composite Rubber Reinforced with Hollow Glass Microsphere Based on Acoustic Finite Element Simulation *Polymers* 15 (3) 2023: pp. 611 – 625. https://doi.org/10.3390/polym15030611
9. **Yang, Z., Hou, P., Jiang, W., Yang, L., Zuo, X., Geng, D., Zhu, Z., Li, H.** Construction of Acoustic Model and Simulation of Sound Absorption Performance of Composite Acoustic Lining for Aero-engines *Journal of Aeronautical Materials* 43 (5) 2023: pp. 84 – 96. https://doi.org/10.11868/j.issn.1005-5053.2022.000151
10. **Ma, Z.** Research on Low-Frequency Noise Reduction Technology Using Flexible Acoustic Metamaterials *North University of China* 2 2023: pp. 77. https://link.oversea.net/doi/10.27470/d.cnki.ghbgc.2023.000384
11. **Qi, M., Liu, L., Chen, Q., Lu, C., Chen, W.** Research on the Acoustic Characteristics of Composite Microperforated Panel Structures Based on Porous Materials *Journal of Shandong University of Science and Technology (Natural Science Edition)* 41 (3) 2022: pp. 83 – 90. https://link.oversea.cnki.net/doi/10.16452/j.cnki.sdkjzk.2022.03.010
12. **Zhang, B., Rong, J., Cheng, X.** Optimization Design of an Acoustic Cover Layer for a Cylindrical Cavity Based on Porous Materials *Chinese Journal of Engineering* 47 (3) 2025: pp. 468 – 479. https://link.oversea.cnki.net/doi/10.13374/j.issn2095-9389.2024.06.07.002
13. **Chen, Y.** Research on the Acoustic Performance of Sandwich Structures Based on Negative Poisson's Ratio Structures *Guangzhou University* 4 2024: pp. 93. https://link.oversea.cnki.net/doi/10.27040/d.cnki.ggzdu.2024.001548
14. **Xiong, X.** Research on Acoustic Performance Testing of Automotive Porous Sound Absorbing Materials *Shanghai University of Engineering Science* 1 2021: pp. 1 – 82. https://link.oversea.cnki.net/doi/10.27715/d.cnki.gshgj.2021.000612
15. **Chen, H., Ou, Y., Liu, Q., He, T., Yang, L., Li, Y.** Simulation of Load-bearing and Vibration Performance of Water-lubricated Tail Bearing System Based on Acoustic Metamaterials *Journal of Ship Engineering* 46 (12) 2024: pp. 11 – 22. https://link.oversea.cnki.net/doi/10.13788/j.cnki.cbgc.2024.12.02
16. **Zu, X., Ren, X., Zou, Z., Li, H.** Acoustic and Vibration Characteristics of Fiber/Resin Sandwich Panels with Porous foam Core *Journal of Air Power* 38 (9) 2023: pp. 2214 – 2220. https://link.oversea.cnki.net/doi/10.13224/j.cnki.jasp.2021063 2
17. **Chen, W., Liu, S.** Analysis and Design Optimization of Sound Absorption Performance of Porous Materials *Noise and Vibration Control* 32 (3) 2012: pp. 177 – 182. https://doi.org/10.3969/j.issn.1006-1355.2012.03.041
18. **Sun, W., Liu, B., Yan, X., Gao, K.** Simulation of Acoustic Properties of Polyurethane/epoxy Resin Elastomers *Functional Materials* 46 (1) 2015: pp. 1099 – 1102. https://doi.org/10.3969/j.issn.1001-9731.2015.01.020
19. **Lv, L., Wen, J., Zhao, H., Wen, X.** The Dynamic Mechanical Properties of Viscoelastic Materials and their Influence on the Sound Absorption Performance of the Covering Layer *Acta Physica Sinica* 63 (15) 2014: pp. 1 – 6. https://doi.org/10.7498/aps.63.154301
20. **Guo, R., Tang, W.B., Zhu, W.W.** Comparison of 1D Transfer Matrix Method and Finite Element Method with Tests for Acoustic Performance of Multi-chamber Perforated Resonator *Applied Acoustics* 112 2016: pp. 140 – 146. https://doi.org/10.1016/j.apacoust.2016.05.018
21. **Chen, J.T., Chen, Y.W.** Dual Boundary Element Analysis Using Complex Variables for Potential Problems with or without a Degenerate Boundary *Engineering Analysis with Boundary Elements* 24 (9) 2000: pp. 671 – 684. https://doi.org/10.1016/S0955-7997(00)00025-4
22. **Su, J., Zheng, L.** Research on the Acoustic Performance Mechanism of a Novel Composite Structure in Vertical Incidence and Diffusion Domains *Journal of Mechanical Engineering* 57 (17) 2021: pp. 149 – 162. https://doi.org/10.3901/JME.2021.17.149
23. **Luo, W., Jiang, J., Liu, Q., Huang, D.** Noise Reduction Study of Train Structure Noise Based on the FE-SEA Hybrid Method *Journal of Railway Engineering* 42 (10) 2020: pp. 113 – 117. https://doi.org/10.3969/j.issn.1001-8360.2020.10.016
24. **Zhang, Y.** Research on the Optimization of Sound Absorption Performance of Foam Metals and Their Composite Structures *Xi'an University of Architecture and Technology* 2022: pp. 1 – 87.

https://link.oversea.cnki.net/doi/10.27393/d.cnki.gxazu.2022.001126

25. **Yang, M., Feng, T., Jia, Y., Wang, J.** Research on a Mixed Calculation Method for the Normal Sound Absorption Coefficient of Foam Materials under Air-backed Conditions *Noise and Vibration Control* 38 (2) 2018: pp. 42 – 76. https://doi.org/10.3969/j.issn.1006-1355.2018.02.009